Specific heat of single-crystal HfV_2: Strong-coupling conventional superconductivity and the effect of the martensitic transition

F. R. Drymiotis, J. C. Lashley, T. Kimura, G. Lawes, J. L. Smith, and D. J. Thoma
Los Alamos National Laboratory, Los Alamos, New Mexico 87545, USA

R. A. Fisher and N. E. Phillips
Lawrence Berkeley National Laboratory and Department of Chemistry, University of California, Berkeley, California 94720, USA

Ya. Mudryk and V. K. Pecharsky
Ames Laboratory and Department of Materials Science and Engineering, Ames, Iowa 50011, USA

X. Moya and A. Planes
Department d'Estructura i Constituents de la Matèria, Universitat de Barcelona, Diagonal 645, 08028 Barcelona, Catalonia, Spain
(Received 16 March 2005; published 28 July 2005)

Specific-heat (C) measurements on single crystals of HfV_2 were made from 1 to 150 K in magnetic fields (B) to 14 T applied along the [110] axis. The type-II superconductor HfV_2 has a martensitic transition at $T_M \sim 118$ K and becomes superconducting at $T_c \sim 8$ to 9 K. Specific heats are thermal-history dependent and T_c increases following repeated cooling cycles from ambient temperature through T_M. This progression is probably related to an incomplete structural transition from cubic-to-orthorhombic symmetry at T_M and the related strains that are produced. Differential scanning calorimetry through T_M had a hysteresis of ~ 1 K related to cooling and warming cycles between 90 and 140 K with no other effect on the martensitic transition. An x-ray determination of phase contents for one sample was used to establish a ratio ($\sim 1:10$) of cubic-to-orthorhombic phases below T_M. Both phases are superconducting, but only a sharp, anomaly is observed at T_c, which can be rationalized if both phases have nearly identical T_c's. From fits to the specific heat above T_c, a representative derived Debye temperature (Θ_D), characterizing the low-temperature lattice specific heat, is 177 K. At T_c the ratio $\Delta C(T_c)/\gamma T_c = 2.07$, with $T_c = 8.00$ K and $\gamma = 42.1$ mJ K^{-2} mol^{-1}, is representative of the specific-heat measurements and indicates strong coupling. This ratio is nearly independent of variations in T_c and C associated with repeated cooling from ambient temperature through T_M. The conventional superconducting state specific heat can be fitted with the alpha model for strong coupling using an energy gap $\Delta(0)/k_B T_c = 2.1$. It has an associated electron-phonon coupling constant $\lambda = 1.45$. Both parameters are similar to those for the type-I superconductor Pb. In the normal state the Sommerfeld constant (γ) depends on the thermal history, with a general increase as T_c increases. For $B > 0$ the superconducting anomaly shifts to lower temperatures and the Sommerfeld constant in the vortex state (γ_v) is linear in B with values and slopes that depend on the thermal history. Extrapolating $\gamma_v(B)$ vs B to γ yields upper critical fields (B_{c2}) ranging from 29 to 35 T.

DOI: 10.1103/PhysRevB.72.024543 PACS number(s): 74.25.Bt, 74.25.Op, 74.62.−c, 81.30.Kf

I. INTRODUCTION

Superconducting transitions are preceded by martensitic transitions in certain compounds with the A15 structure (V_3Si, Nb_3Sn, V_3Al),[1,2] C15 Laves phase structure (HfV_2, ZrV_2),[3–5] and in the B2 cesium chloride structure (VRu).[6] They are all cubic at ambient temperature. Below the martensitic transformation temperature (T_M) the A15 and B2 materials become tetragonal, while the C15 materials transform into orthorhombic or rhombohedral structures. The C15 Laves phase intermetallic HfV_2 transforms from a cubic (C15, AB_2 structure) to an orthorhombic (A15, O_h^3 symmetry structure) at $T_M \sim 118$ K and exhibits extraordinary resilience to neutron-radiation damage.[7] At cryogenic temperatures it becomes a type-II superconductor, with $T_c \sim 8$ to 9 K, and critical magnetic field, $B_{c2} \sim 30$ T. In addition to its resistance to neutron-radiation damage, the material softens with decreasing temperature[8] making plastic deformation possible at cryogenic temperatures.[9] Although HfV_2 has been studied for over 30 years, the influence of microstructure on the nature of the martensitic transition and controversy over whether the superconductivity is conventional or unconventional continues to make it an interesting material.

Our goals for the research reported in this paper were fourfold: first, to use specific-heat (C) measurements to show how the martensitic transition is coupled to and affects the superconductivity and second, to obtain the entropy (ΔS_M) and enthalpy (ΔH_M) of the phase transformation; third, to identify the nature of the superconductivity; and fourth, to track the evolution of the Sommerfeld constant in the vortex state (γ_v) with magnetic field (B). All previous measurements[10–16] of specific heat used polycrystalline samples, or crystals with high mosaicity, in zero magnetic fields. In this paper we report temperature and magnetic field dependent specific-heat measurements on two single crystals, and on two polycrystalline samples for $B = 0$.

TABLE I. Parameters that characterize the superconducting and normal properties of HfV_2 single crystal sc1 for $B=0$ are listed as a function of the cooling sequence from ambient temperature (except where noted) through the martensitic transition at $T_M=117.6$ K. The last entry in the table is for a second single crystal sc2 with the same T_M as sc1. The table units are in mJ, K, and mole HfV_2.

Cooling sequence	T_c (K)	γ	γ_r	B_3	Θ_D (K)	$B_5\times10^3$	$\Delta C(T_c)/k_BT_c$	λ
LBNL (sc1-1)[a]	8.00	42.1	0.5	1.090	177	−3.810	2.07	1.45
LANL (sc1-1)[a]	7.78	44.8	0.9	1.078	176	−3.235	2.06	1.61
LANL (sc1-2)[a]	8.45	47.4	0	1.176	171	−4.630	2.04	1.76
LANL (sc1-3)[a]	8.76	46.2	1.0	1.256	167	−5.440	2.10	1.69
LANL (sc1-4)[a]	8.7[d]	46.7	—	1.213	169	−4.985	—	1.72
LANL (sc1-5)[a]	8.60	45.9	1.2	1.198	170	−4.939	2.05	1.67
LANL (sc1-6,7,8,9,10)[b]	9.00	53.8	2.4	1.069	176	−3.773	1.95	2.13
LANL (sc2-1,2,3,4)[c]	8.10	44.4	1.0	1.068	176	−3.698	1.99	1.58
							⟨2.04⟩	⟨1.70⟩

[a]LANL sc1-1 was cooled at 20 K min^{-1}, LANL sc1-2,3,4 at 2 K min^{-1}, and LANL sc1-5 at 0.01 K min^{-1}. The LBNL sc1-1 first stage of cooling was achieved by establishing contact between the sample and a 77 K heat sink using 2×10^{-4} torr nitrogen gas and mechanical heat switches. The cooling rate was approximately exponential and <1 K min^{-1} near T_M. From 77 to 4.2 K the sample was in contact with liquid helium only through mechanical heat switches, and cooled to 4.2 K in ~4 h.

[b]Following the specific-heat measurements for sc1-6 to 150 K there were four additional cycles of cooling from and measurement to 150 K, with no intermediate warming to ambient temperature. To within experimental accuracy all of the specific heats for the five measurements were identical and were analyzed collectively.

[c]The initial cooling of LANL sc2-1 for the first specific-heat measurement was from ambient to 2 K. Three additional specific-heat measurements, with cooling cycles from 150 K and no intermediate warming to ambient temperature, were made following this measurement. The specific heats for all four measurements coincided to within experimental accuracy and were analyzed collectively.

[d]T_c is for 0.5 T. No measurements of specific heat were made for $B=0$ because of a PPMS failure; however, as observed in LANL-3 sc1, the decrease of T_c from $B=0$ to 0.5 T is <0.1 K.

II. EXPERIMENT

Single-crystal HfV_2 was made using the optical-floating-zone technique. As a first step, Hf (99.9%) and V (99.9%) in the molar ratio 1:2 were melted together in an arc furnace in an Ar atmosphere. Several polycrystalline buttons were prepared in this manner, and then combined in an arc furnace under Ar to form the feed rods for the optical-floating-zone furnace. The growth took place under an ultrahigh-purity Ar flow with the growth rate fixed at 6 mm h^{-1}. The resulting sample was cylindrically shaped, ~2 cm in length, and 1 cm in diameter. X-ray powder diffraction measurements showed sharp Bragg peaks and a single-phase pattern corresponding to the cubic Cu_2Mg structure. Laue patterns, taken on disk-shaped samples cut from the cylinder, confirmed its single-crystalline nature. From those patterns the preferred growth axis was deduced as [110]. Laue patterns taken in an area defined by a radius of ~0.2 cm from the center of the sample showed the same orientation, whereas patterns taken closer to the cylinder's edge showed deviations from [110] alignment. It was concluded that the cylindrical sample consisted of large, single-crystal grains with the same orientation confined within a cylindrical volume of radius ~0.2 cm centered on the core of the cylinder.

Measurements of specific heat were made on single crystals (sc1 and sc2) and polycrystalline samples (pc1 and pc2) with $B\|[110]$. The measurements at Los Alamos National Laboratory (LANL) were done with a physical properties measurement system (PPMS) and at Lawrence Berkeley National Laboratory (LBNL) using a semiadiabatic, heat-pulse technique. The LBNL sc1 sample had a mass of 0.65 g from which a smaller piece of mass ~0.06 g had been cut previously for the LANL measurements. Combined experiments at LBNL and LANL for these samples covered the temperature (T) range 1 to 150 K in magnetic fields to 14 T applied parallel to the [110] crystallographic direction. Cooling rates for sample sc1 are given in Table I. All samples were field cooled prior to the specific-heat measurements. (In a separate experiment, two specific-heat measurements were made in 8 T: first, with 8 T applied after the sample had been cooled to 2 K from 150 K in zero field; second, after cooling to 2 K from 150 K in 8 T. There were no observable differences in the two data sets.)

A third single-crystal (sc3) was used for temperature-dependent x-ray powder diffraction measurements[17] to determine the ratio of cubic-to-orthorhombic phases for $T<T_M$ and the lattice parameters. The temperature range was 20 to 300 K for $B=0$.

The martensitic transition was also studied using differential scanning calorimetry (DSC) to test for reproducibility and hysteresis in the transition for cooling/warming cycles. Measurements were done with a high-sensitivity calorimeter capable of working under applied magnetic fields to 5 T.[18] The time constant for the calorimeter is <10 s. The sample was a single crystal (sc4) of mass 0.06661 g.

The text, figures, and tables use the identifiers [LBNL sc1-1 or LANL sc*i*-*n*], where *i* is used to designate the single-crystal sample and *n* is the number of times it was cooled through T_M. Similar identifiers [LANL pc*i*-*n*] are used for the polycrystalline samples.

TABLE II. Lattice parameters and phase volumes (V) for HfV_2, measured as T was decreased from ambient temperature, during the first cooling through T_M, tabulated as a function of temperature. Above the martensitic transition only the cubic phase is present. In the predominantly orthorhombic (ortho) phase below T_M there is ~9 wt % of the untransformed cubic phase.

T (K)	a (Å) [cubic]	V (Å^3) [cubic]	a (Å) [ortho]	b (Å) [ortho]	c (Å) [ortho]	V (Å^3) [ortho]
20	7.329(2)	393.7(2)	5.1730(5)	5.2160(4)	7.4051(8)	199.81(4)
30	7.329(2)	393.7(2)	5.1738(5)	5.2167(4)	7.4033(8)	199.81(4)
40	7.332(2)	394.1(2)	5.1743(5)	5.2164(4)	7.4051(7)	199.87(3)
60	7.334(2)	394.5(2)	5.1813(6)	5.2145(4)	7.3998(8)	199.93(4)
80	7.339(2)	395.3(2)	5.1883(7)	5.2133(5)	7.3943(9)	200.00(4)
90	7.341(2)	395.6(2)	5.1919(8)	5.2124(5)	7.3910(8)	200.02(4)
95	7.342(2)	395.8(2)	5.1942(10)	5.2109(6)	7.3892(9)	200.00(4)
130	7.3690(2)	400.15(1)	—	—	—	—
140	7.3698(2)	400.28(1)	—	—	—	—
150	7.3709(2)	400.46(1)	—	—	—	—
200	7.3781(2)	401.64(1)	—	—	—	—
250	7.3857(2)	402.888(1)	—	—	—	—
300	7.3957(2)	404.52(1)	—	—	—	—

III. MEASUREMENTS AND RESULTS

A. Martensitic and superconducting transitions

The martensitic transition at T_M has been reported to involve two closely spaced structural modifications from cubic to tetragonal to orthorhombic in the range 100 to 115 K.[19] It is not complete, and at low temperatures there is a mixture of untransformed cubic and predominantly orthorhombic phases whose composition depends on the thermal history.[16,18–20]

One paper[20] reported that a polycrystalline sample of HfV_2 was cooled to a bulk superconducting phase in an untransformed cubic structure with a transition temperature $T_c = 8.1$ K, which led to the conclusion that the superconductivity is not significantly influenced by the crystallographic structure. Since there is a wide variation in T_c, depending on the thermal history, it would not be unreasonable to anticipate two anomalies, or at least a significant broadening of a single anomaly, for a mixed-phase sample. However, there is only one, relatively sharp, T_c with a transition width $\Delta T_c \sim 1$ K for all samples measured in this research, or for those reported previously by others. This can be rationalized if both phases have essentially the same T_c and are influenced in the same way by the thermal history.

B. X-ray measurements

X-ray powder diffraction measurements showed that the transition from the cubic to the orthorhombic phase at T_M was incomplete, which will create grain boundaries and strains in the lattice that are probably related to the thermal-history dependence of, e.g., T_c, γ, and γ_v—Secs. III C and III D—where γ and γ_v are, respectively, the electronic specific heat in the normal and vortex states. (The possibility of fracturing and/or micro-cracking at T_M as a contributor to the variability in these parameters was eliminated through elastic-constant measurements that were made on a single crystal following an initial cooling from ambient temperature through T_M. Those measurements would not have been possible if the single crystal had cracked or fragmented. Furthermore, it is well known that most martensitic transitions do not cause breakup of the sample.)

The x-ray determinations of the lattice parameters were made on sample sc3—ground into a powder and mixed with GE7031 varnish—from 300 to 20 K (see Table II) during the first cooling from ambient temperature. (The orthorhombic a axis increased with increasing T while the b and c axes decreased. For the cubic phase the a axis increased with increasing T.) Two additional measurements were made at 140 and 40 K following cycles between those temperatures. The particle length below T_M was estimated at 1 to 5×10^{-6} m based on the absence of line broadening. Only the cubic structure was present at 140 K, but below T_M both orthorhombic and ~9 at. % untransformed cubic phases were present—independent of the number of cooling cycles. For a fixed T the a axis for the cubic phase and the a and b axes for the orthorhombic phase were not dependent on the number of cooling cycles; however, the c axis for the orthorhombic phase increased monotonically for each passage through T_M. Presumably, different samples, or possibly the same sample following additional cooling cycles from ambient temperature, could have different ratios of cubic-to-orthorhombic phases. This ratio probably also depends on the physical state of the sample—powder, polycrystalline, or single crystal.

C. Specific-heat measurements for $B=0$

We report first on the PPMS measurements made on single crystal sc1 at LANL. Figure 1 is a plot of C/T vs T from 1.8 to 135 K for $B=0$, which was measured following the second cooling of the sample through T_M from ambient temperature. This was the only specific-heat measurement made to temperatures above T_M. The superconducting (SC)

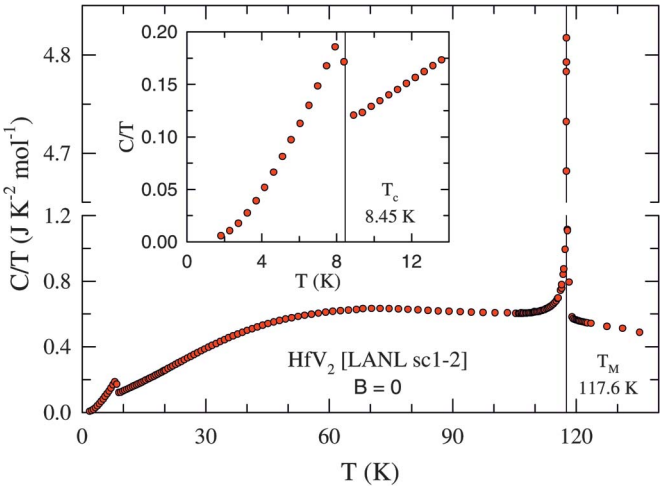

FIG. 1. (Color) C/T vs T for HfV_2 for the smaller piece cut from single crystal sc1 showing the martensitic and superconducting transitions. (To display the high, narrow anomaly at T_M =117.6 K the C/T scale is split into two sections.) The inset shows an expanded region of C/T vs T in the vicinity of T_c with an entropy conserving construction at 8.45 K.

transition at T_c=8.45 K is in marked contrast to T_c=7.78 K following the first cooling from ambient temperature and measurements of specific heats in B=0 and 8 T from 2 to 15 K. A total of six specific-heat measurements were made on the LANL sc1 sample following successive cooling through T_M from ambient temperature, with an additional four made after repeated cooling from 150 K. The results clearly show that parameters characterizing the specific heat are dependent on the thermal history of the sample.

Figure 2 illustrates how T_c for B=0 depends on thermal cycling. When the sample is successively cooled from ambient temperature T_c increases; however, when cooling is from 150 K there is no effect on T_c. Other parameters affected by the thermal history are the specific heat of the lattice (C_{lat}), the normal (γ) and vortex [$\gamma_v(B)$] states, and, a small residual Sommerfeld constant (γ_r) that is probably due to an electron density of states (EDOS) in a normal phase mixed with the majority superconducting phase of the sample. (Severe strains in small regions of the sample could completely quench superconductivity and lead to occlusions of normal material whose presence is indicated by γ_r.) There is a general increase in γ (an increase in EDOS) linked to the increase in T_c.

Specific heats for sample sc2 were measured at LANL from 1 to 150 K following an initial cooling from ambient temperature and four subsequent cooling cycles from 150 K. These measurements were made to test the effect of repeated cooling from 150 K through T_M. To within experimental accuracy all of the data coincided with a T_c=8.1 K.

Polycrystalline sample pc1 was measured for B=0 from 2 to 150 K. A second polycrystalline sample (pc2) was measured in B=0 to test the effect on the specific heat after cooling to 2 K from ambient temperature followed by three

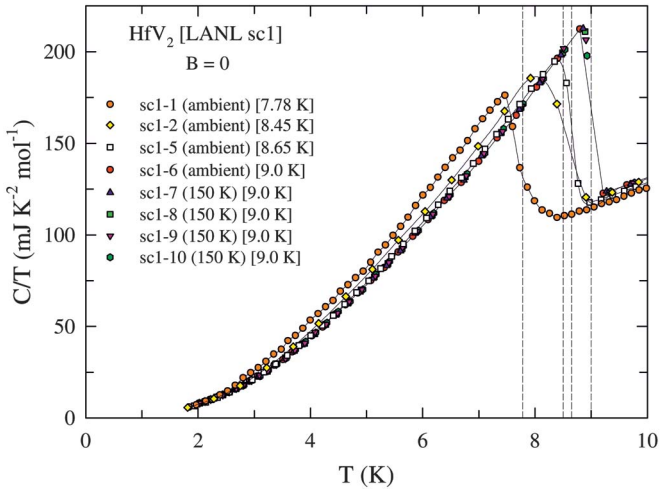

FIG. 2. (Color) A plot of C/T vs T for the smaller piece cut from HfV_2 single crystal sc1. (In the legend the temperatures given in parentheses are the initial temperatures at the start of the cooling sequence.) The results demonstrate changes in the specific heat in the vicinity of the superconducting transition as a function of the thermal history. There is a progressive increase in T_c and C changes for successive cooling sequences started at ambient temperature. For cooling cycles initiated at 150 K, both T_c and C are unchanged.

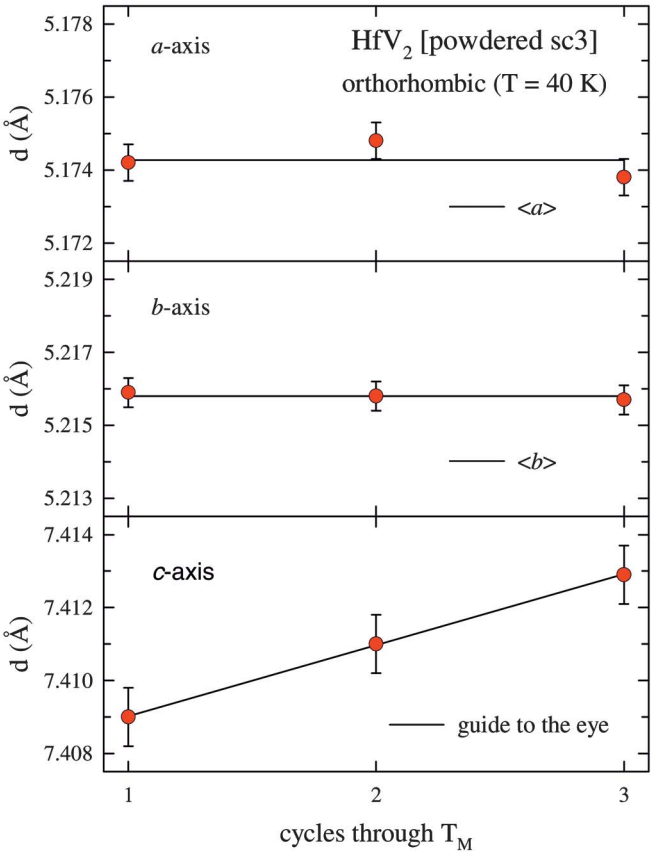

FIG. 3. (Color) A plot of the lattice parameters at 40 K for the orthorhombic phase of HfV_2, containing ~9 wt % untransformed cubic phase, as a function of the number of cooling cycles through T_M (see text). Successive cycles produce a monotonic increase in the c axis while the a and b axes are unaffected. For the vertical scales the number of increments and their spacing is the same for each axis.

TABLE III. The parameters characterizing the superconducting and normal properties of polycrystalline HfV_2 for $B=0$ are listed in chronological order from previously reported specific-heat measurements (unspecified thermal history) and include, as the last table entries, two samples from the present research after the first cooling sequence from ambient temperature. The table units are in mJ, K, and mole HfV_2.

T_M (K)	T_c (K)	γ	$B_3\times10^3$	Θ_D (K)	$B_5\times10^3$	$\Delta C(T_c)/k_BT_c$	λ	Refs.
—	8.4	57.0	—	190	—	1.7	2.3	10
118	—	—	—	—	—	—	—	11
114	8.85	53.7	—	—	—	—	2.1	12
118	9.0	58.1	1.17	170	−4.075	1.9	2.4	13
—	9.2	47.7	1.13	173	−2.760	2.0	1.8	14
117	9.0	50.0	—	—	—	1.8	1.9	15
117	9.1	51.6	1.23	165	−4.161	1.85	2.0	16
96.3	7.60	55.8	1.385	162	−5.479	1.95	2.25	pc1
100[a]	9.00	60.4	1.245	167	−4.244	1.93	2.51	pc2

[a]Three additional cooling cycles were made from 150 to 2 K—with no intermediate warming to ambient temperature—following the first from ambient temperature. The specific-heat measurements for all four coincided to within experimental accuracy.

additional cooling cycles through T_M from 150 K. This was analogous to the test made with single crystal sc2 and gave similar results.

Various parameters characterizing the specific heat for sc1 and sc2 are collected in Table I. For comparison, parameters reported previously by others for polycrystalline samples, and those for pc1 and pc2, are also listed in Table III.

D. Thermal-history dependence of T_c

As sample sc1 was successively cooled from ambient temperature through T_M to low temperatures, T_c *increased* as shown in Fig. 2 and Table I; however, successive cooling cycles from 150 K had no effect. It is tempting to associate these increases in T_c with a change of the ratio of cubic-to-orthorhombic phases below T_M. However, this would be possible only if repeated cooling from *ambient* temperature—but not from 140 to 150 K—can reduce the ratio.

However, since both phases are superconducting, with essentially the same specific heat, it is assumed that the mechanism for changes in T_c must be associated with strains originating from the incomplete structural conversion at T_M. It seems reasonable to assume that the degree of strain is proportional to the amount of cubic phase below T_M. (The x-ray measurements showed that only the cubic phase was present at 140 K.) Since subsequent cooling through T_M from 140 to 150 K did not change either T_c or the ratio of cubic-to-orthorhombic phases, the conclusion is that the strains did not change. It is hypothesized that warming to ambient temperature relieves the strains and "trains" the sample so that each additional cooling cycle through T_M progressively decreases the ratio of cubic-to-orthorhombic phases and/or strains.

The lack of change in T_c when cooling from 140 to 150 K through T_M implies that the reduction of strain is an activated process. Strain-driven increases in the orthorhombic c axis with repeated cycling through T_M (see Fig. 3) might provide a means for their reduction. A proposed mechanism would require the orthorhombic phase to retain a "memory" of the c-axis increase following cooling through T_M, and the "training" would be identified with the monotonic increase in the c axis. However, for this mechanism to operate requires that cooling through T_M must first be preceded by a return to ambient temperature, which is the activation part of the process. For this scenario, each additional sequence of cooling from ambient temperature through T_M produces a *decrease* in strains and an *increase* in T_c. (It is assumed, *a priori*, that a decrease in strain will increase T_c.)

E. Specific-heat measurements for $B>0$

Three sets of specific-heat measurements were made at LANL on sample sc1 in fields to 14 T after the third, fourth, and fifth cooling sequences. The results for the fifth sequence are shown in Fig. 4 as C/T vs T from 1.9 to 12 K for $B=0$ to 14 T along the [110] crystal axis; results for the third and fourth sequences are similar.

Only a single cooling through T_M—the first cooling of the large sc1 sample—was done for the LBNL measurements. Those specific-heat measurements covered the range 1 to 20 K and $B=0$, 5, and 9 T and are displayed in Fig. 5. The widths of the transitions, particularly for $B>0$, are relatively greater than those of the smaller piece measured at LANL. This could be a consequence of greater strains in the larger piece induced at the martensitic transition. In the case of the in-field measurements, it might also indicate misalignment differences of B with the [110] axis for the two samples. The data for $B=0$ are given in Table I.

F. Specific-heat measurements in the vicinity of T_M

The specific-heat data in the vicinity of T_M are shown in Fig. 6 for polycrystalline sample pc1 and single-crystal sample sc1, both measured at LANL. T_M is 117.6 K for the single crystal, as defined by an entropy-conserving construction, with the transition extending over ~10 K, as shown by the enhanced specific heat above and below T_M. This broadening of the specific-heat anomaly reflects the series of struc-

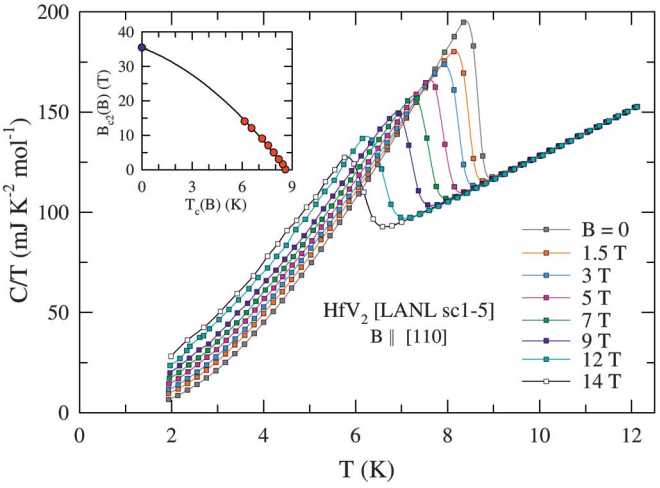

FIG. 4. (Color) Plot of C/T vs T as a function of magnetic field showing a typical evolution of the superconducting transition temperatures and anomalies as B is increased from 0 to 14 T. Curves through the data are guides to the eye. The inset shows a plot of $B_{c2}(B)$ vs $T_c(B)$ where $T_c(B)$ was obtained from entropy conserving constructions for $B \leqslant 14$ T. $B_{c2}(0)$ at $T_c=0$ was obtained from the linear extrapolation of $\gamma_v(B)$ versus B shown in Fig. 15. The curve represents a quadratic fit to the data.

tural modifications reported in Ref. 19, which extend over a comparable range of temperature. Although martensitic transitions are first order, the shape of the anomaly is lambdalike (unlike any previously reported), which resembles a second-order transition.

In contrast to the single crystal, the martensitic transition at $T_M=96.3$ K for polycrystalline sample pc1 is sharper with a width of ~1 K and a shape that is suggestive of a first-order transition. Previously reported specific-heat measurements[11–13,15,16] on polycrystalline samples have similar transitions, but with T_M ranging from 114–118 K, which is comparable to that for single crystal sc1. Although the

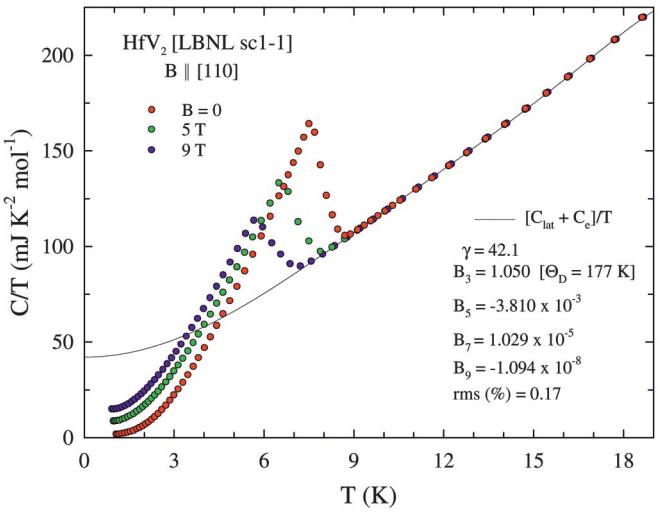

FIG. 5. (Color) A plot of C/T vs T from $B=0$ to 9 T showing the result of the least-squares fit used to evaluate the lattice and normal electronic state (EDOS) specific heats. The fit parameters are listed in the figure.

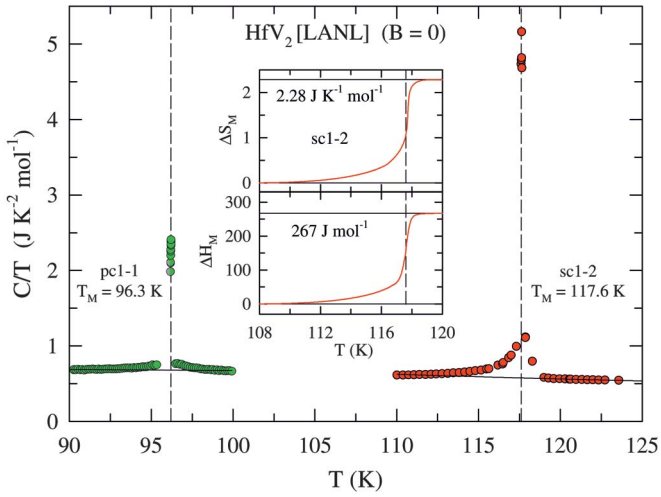

FIG. 6. (Color) A plot of C vs T in the vicinity of T_M shows the contrasting martensitic transitions for a polycrystalline (pc1) and a single-crystal (sc1) sample of HfV_2. The solid curves are from polynomial fits to the data, well above and below T_M, to establish "baselines" to be used in calculating ΔH_M and ΔS_M for the transitions, which are shown for LANL sc1-2 in the inset.

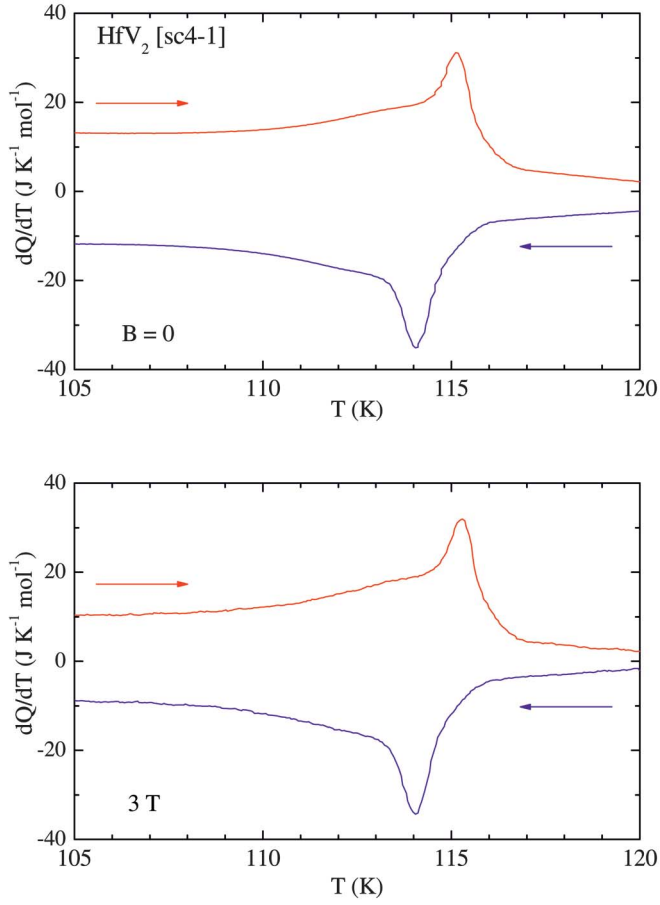

FIG. 7. (Color) DSC curves in the vicinity of the martensitic transition at ~115 K in applied fields of $B=0$ and 3 T for sample sc4. Arrows indicate the cooling and warming curves. The sharper peak is probably related to the cubic-to-orthorhombic transition and the long decay is a signature of an incomplete conversion of the cubic phase to the orthorhombic phase.

polycrystalline sample pc1 has $T_M \sim 21$ K lower in temperature than the single crystals it is superconducting. However, $T_c = 7.60$ K is the lowest reported value and there is a large $\gamma_r = 11.7$ mJ K^{-2} mol^{-1}. The second polycrystalline sample, pc2, has $T_M = 100$ K (also low), with $T_c = 9.0$ K, and $\gamma_r = 2.3$ mJ K^{-2} mol^{-1}. Over an extended range above T_c, the specific heats for samples pc1 and pc2 are essentially the same to within experimental accuracy.

The homogeneity range of HfV_2 is only a few percent, and there is a sharp dependence of the composition of a solid on temperature just below the melting point. A possible explanation of the lower T_M's for the polycrystalline samples may be that their stoichiometry is slightly different compared to that of the single crystals.

An analysis of the single-crystal, specific-heat data for sc1 shown in Fig. 6 was made in the vicinity of T_M to determine the enthalpy (latent heat) (ΔH_M) and entropy (ΔS_M) changes associated with the transition. A least-squares polynominal fit was made to the data from well above and below the transition region to obtain a "background" specific heat (C_{bkg}). Integration of $(C - C_{bkg})$ and $(C - C_{bkg})/T$ with respect to T gave $\Delta H_M = 267$ J mol^{-1} and $\Delta S_M = 2.28$ J K^{-1} mol^{-1}, respectively. Since an unknown amount of untransformed cubic phase is present below T_M, actual values would be larger—by $\sim 9\%$, perhaps, based on the x-ray determination of the phase content of sample sc3-1.

A similar analysis was made for the pc1 data shown in Fig. 6, which gave $\Delta H_M = 117$ J K^{-1} and $\Delta S_M = 1.22$ J K^{-1} mol^{-1}. These values are $\sim 1/2$ those for the single crystal, which implies that either $\sim 50\%$ of the polycrystalline sample is in the cubic phase below T_M or is in a phase where the martensitic transition has been suppressed. Values of ΔH_M and ΔS_M were not determined for sample pc2.

Three additional cooling cycles for pc2 from 150 to 2 K, without return to ambient temperature, had no effect on C. If the assumption is correct that larger T_c's are associated with less untransformed cubic phase and/or lower strain, then pc2-1 with $T_c = 9.0$ K has less cubic phase and/or strain for the initial cooling than either of the single crystals or pc1.

G. DSC measurements near T_M

The reproducibility of the martensitic transition at T_M was checked using DSC to measure warming and cooling thermograms between 90 and 140 K in magnetic fields to 5 T. Thermograms record the evolution of the transition temperature. The warming and cooling scan rates were 0.017 K s^{-1}. Since the time constant for the apparatus is <10 s the temperature was retarded by <1 K. Examples of the thermograms for fields of $B = 0$ and 3 T are shown in Fig. 7. For all cases, the curves show a peak followed by a long decay. The existence of such a long decay is characteristic of systems for which the martensitic transition does not proceed to completion on cooling through T_M because of the production of internal strains that oppose the transformation. Probably, some of this decay is also related to the conversion of the intermediate tetragonal phase to the low-temperature orthorhombic phase.

The temperature range $\Delta T_M \sim 9$ K over which the transition takes place and the hysteresis $\Delta T_h \sim 1$ K (defined as the difference in temperature of the calorimetric peaks for heating and cooling) are independent of B to within the accuracy of the data. The results are shown in Fig. 8. Since it is unlikely that a martensitic transition would be dependent on magnetic field, in the absence of a simultaneous change of magnetic order, any observed changes must be due to the number of thermal cycles that are associated with the changes of B at 140 K. The lack of a thermal-history dependence of T_M from the DSC measurements between 90 and 140 K is similar to that found for both the x-ray and conventional specific-heat measurements that were made following cycling through T_M from 140 and 150 K, respectively—see above.

IV. ANALYSIS AND DISCUSSION

A. The lattice and electronic specific heat

Analysis of the specific-heat data in the superconducting region to determine γ and C_{lat} utilized least-squares fitting of the data above $T_c(B)$ simultaneously for all B to the expression

$$C = \gamma T + \Sigma B_n T^n, \tag{1}$$

where the series $B_n T^n$, with coefficients B_n, is the harmonic-lattice approximation for C_{lat} with $n = 3$, 5, 7, 9 and a fitting range of ~ 9 to ~ 18 K. The electronic specific-heat component (C_e) is obtained by subtracting C_{lat} from C. In the plot of C/T vs T for the LBNL measurements shown in Fig. 5, the curve is the fit $\gamma + C_{lat}/T$. From the coefficient B_3 the characteristic Debye temperature (Θ_D) is calculated from the relationship

$$\Theta_D = [12\pi^4 R N_a / 5 B_3]^{1/3}, \tag{2}$$

where R is the gas constant and N_a the number of atoms in a formula unit. For the LBNL sc1-1 measurement $\Theta_D = 177$ K. For the six measurements made at LANL, Θ_D ranged from 167 to 176 K. Values of Θ_D were 162 and 167 K for polycrystalline samples pc1 and pc2, respectively. Previously polycrystalline samples[10,13,14,16] had reported Θ_D's that varied from 165 to 190 K. These variations in the lattice specific heat are compelling evidence that it is strongly dependent on thermal history and/or the ratio of cubic-to-orthorhombic phases. The first time the LANL and LBNL sc1 samples were cooled the rates were very different—see Table I. Since the Θ_D's are nearly identical, it appears that the *number* of times cooled from ambient temperature is much more significant than the *cooling rate* in determining the low-temperature lattice properties.

For $T = T_c$ there is the thermodynamic requirement that the entropy of the superconducting state, $S_{es} = \int (C_{es}/T) dT$, be equal to the entropy in the normal state, $S_{en} = \gamma T_c$. (C_{es} is defined as the specific heat of the superconducting state.) Using the parameters obtained from a fit to Eq. (1), where γ is an evaluated parameter, will generally not result in equality of the two entropies. To achieve the required balance, a series of fits are made with γ constrained, which is system-

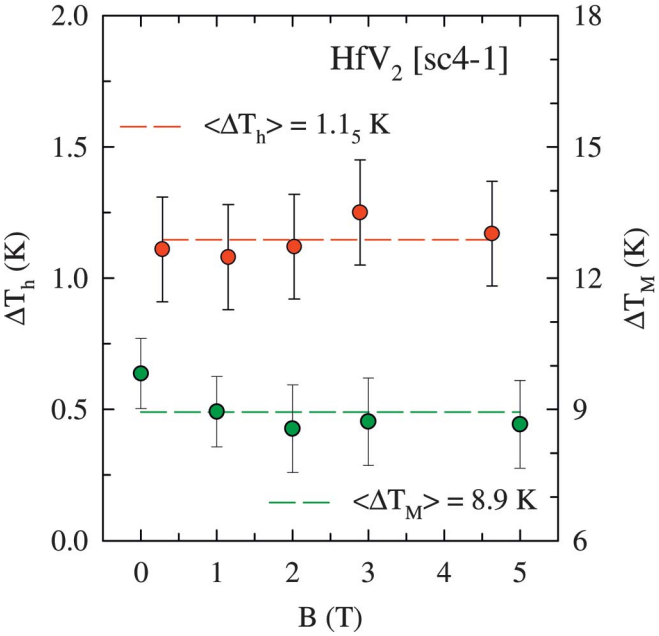

FIG. 8. (Color) This figure shows the temperature range over which the martensitic transition extends (ΔT_M) and the cooling/warming hysteresis (ΔT_h) as a function of magnetic field. Since the martensitic transition for HfV_2 is not expected to have a dependence on magnetic field, the plot actually shows the effect on the transition of the number of cycles—covering the range 90 to 140 K—through T_M. To within experimental error ΔT_M and ΔT_h are independent of the number of cycles and the dashed lines represent the respective average values.

atically varied in an iterative procedure for successive fits, until $S_{es}=S_{en}$. Figure 9 is a plot of C_e/T vs T for the LBNL sc1-1 data; Fig. 10 is a comparable plot for the LANL sc1-5 sample after the data plotted in Fig. 4 were analyzed in a similar fashion. Before an entropy check can be made, the specific heat must be extrapolated to $T=0$; this procedure is

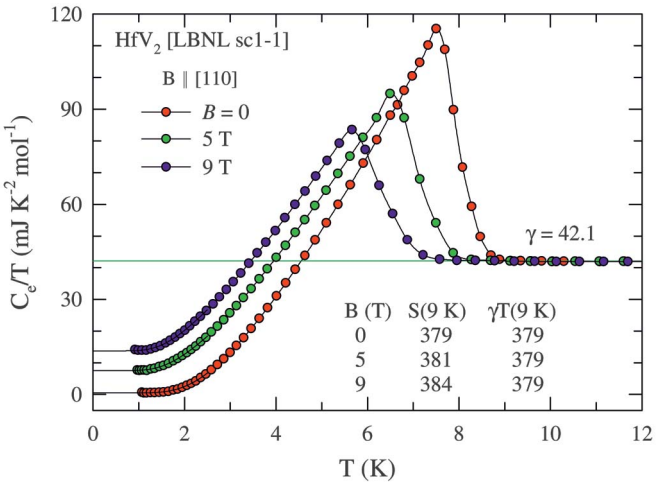

FIG. 9. (Color) The electronic specific heat plotted as C_e/T versus T at $B=0$, 5, and 9 T, which was derived by subtracting the lattice contribution given in Fig. 5. Entropy comparisons are tabulated in the figure for the superconducting and normal states at 9 K. The extrapolated curves below ~1 K are from the fits shown in Fig. 13.

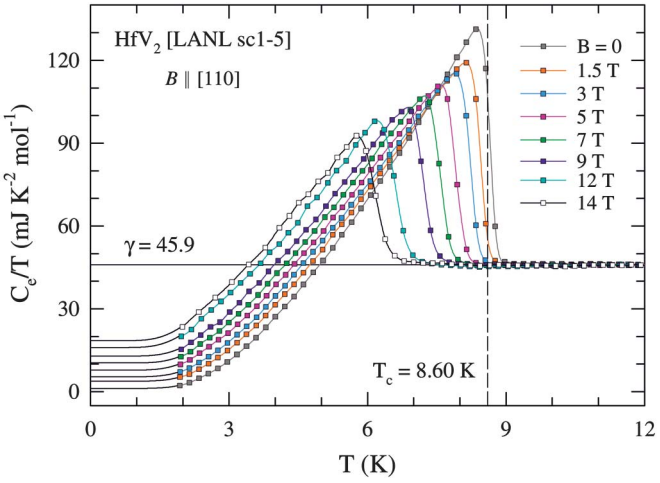

FIG. 10. (Color) A plot of C_e/T vs T in fields to 14 T is shown for the LANL sc1-5 measurements, which is similar to that of Fig. 9 for the LBNL sc1-1 measurements.

described below. The amount of entropy involved in the extrapolation is a small fraction of that at T_c.

B. Nature of the superconductivity: conventional or unconventional

It has been reported[14,16] that the specific heat below T_c follows a T^3 dependence, which was cited as evidence for an anisotropic, superconducting energy gap that vanishes at nodes (points) on the Fermi surface—a possible unconventional p-wave superconductor. Figure 11 is a plot of C_e/T^3 vs T at $B=0$ for the LBNL data shown in Fig. 9. Below T_c the ratio C_{es}/T^3 is nearly constant to ~4.5 K, but for lower temperatures there is a rapid departure from this T^3 dependence.

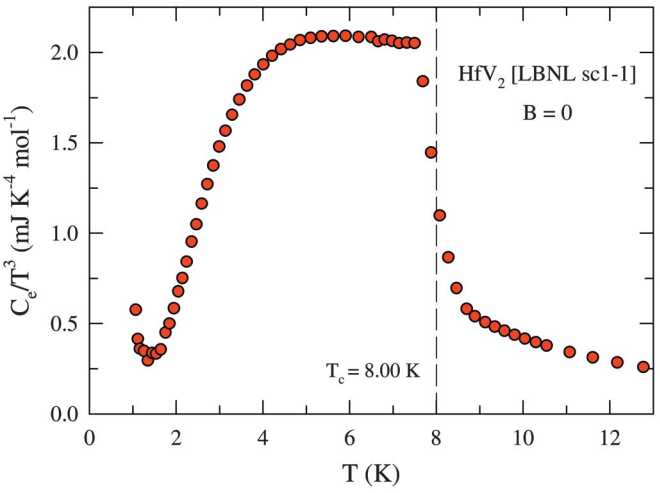

FIG. 11. (Color) A plot of C_e/T^3 vs T for the $B=0$ data shown in Fig. 9. This plot demonstrates the T^3 behavior of C_{es} below T_c to ~4.5 K, which is characteristic of strong coupling. Below this temperature there is a rapid decrease that will be shown to be exponential in Fig. 12. The upturn below ~1.5 K is due to an electron density of states (EDOS) from a small amount of nonsuperconducting, normal material.

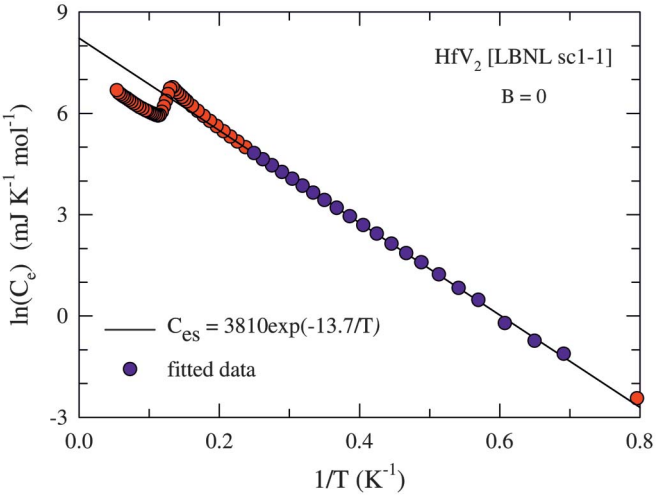

FIG. 12. (Color) A plot of $\ln[C_e]$ vs $1/T$ shows the exponential dependence of C_{es} below ~4.5 K, where the specific-heat data are those for $B=0$ shown in Fig. 9. The departure of the data from the fit line below ~1.4 K is the result of a lowered precision of C_{es} as T approaches zero.

(The upturn in C_{es}/T^3 for $T<1.5$ K is a consequence of an EDOS from a small amount of normal material—see the analysis below.) This plot demonstrates conclusively that HfV_2 is *not* an unconventional superconductor; the T^3 behavior, over a limited region, just below T_c, is not unusual and is related to strong electron-phonon coupling. (Strong coupling was proposed previously for a polycrystalline sample.[13])

Figure 12 is a plot of $\ln C_e$ vs $1/T$ for the LBNL measurements for $B=0$ that show an exponential dependence of C_{es} below ~4 K. The BCS theory[21,22] predicts that at sufficiently low temperatures $C_{es}=a(0)\gamma T_c \exp[-b(0)T_c/T]$, where the region of validity is usually divided into two sections—$2.5 \leqslant T_c/T \leqslant 6$ and $7 \leqslant T_c/T \leqslant 12$—each with different values of the parameters $a(0)$ and $b(0)$. At limiting low temperatures C_{es} for $B=0$ and C_{ev} for the in-field, vortex-state specific heat can be fit by non-linear, least squares to the expression

$$C_{ex}(B) = \gamma(B)T + \alpha(B)\exp[-\beta(B)/T], \qquad (3)$$

where $\alpha(0) \equiv a(0)\gamma T_c$, $\beta(0) \equiv b(0)T_c$. $C_{ex}=C_{es}$ for $B=0$ and C_{ev}, the vortex-state specific heat, for $B>0$. For the LBNL sample sc1-1, in the range $T_c/T=2$ to 5.6 (see Fig. 13), $a(0)=11$ mJ K^{-1} mol^{-1} and $b(0)=1.71$ K, which are comparable to the BCS values 8.5 mJ K^{-1} mol^{-1} and 1.44 K, respectively. Similar values are obtained for the LANL sc1-5 measurements although the fit range is truncated to $T_c/T=2$ to 4 because the measurements are limited to ~2 K. Equation (3) is also used to extrapolate $C_e(B)$ to $T=0$, albeit without theoretical justification. The results of the fits and extrapolations for the LBNL and LANL data are shown in Figs. 13 and 14, respectively, where the fit parameters are tabulated. Gap parameters $\beta(B)$ and prefactors $\alpha(B)$ both decrease with increasing B. For both sets of measurements the entropies above T_c agree for all B to within experimental accuracy as required by the third law of thermodynamics. The entropy checks for the LBNL data for sample sc1-1 are given in Fig. 9.

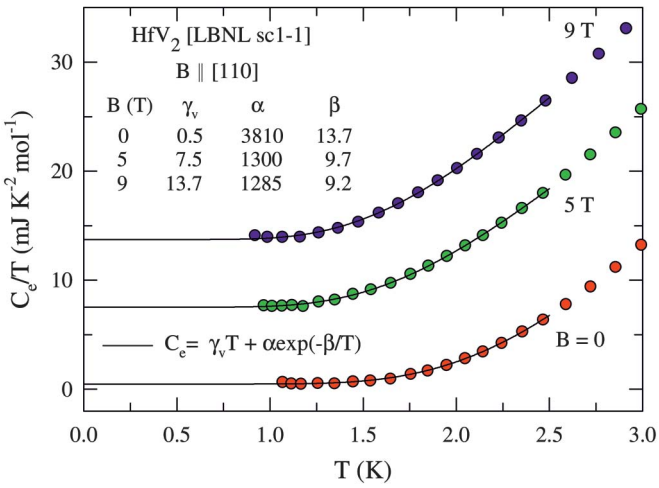

FIG. 13. (Color) A plot of C_{es}/T vs T for $B=0$, 5, and 9 T, which illustrates the results of an exponential fit and extrapolation of the electronic specific-heat data shown in Fig. 9. The fitting expression and parameters are given in the figure.

C. Sommerfeld constant γ vs B and the upper (B_{c2}) and lower (B_{c1}) critical fields

The simplest explanation for a residual linear in T term for $B=0$ is the presence of an EDOS from normal material, which is characterized by a Sommerfeld constant γ_r. All γ_r's for the single-crystal measurements on sc1 and sc2 were small (varying from 0 to 2.4 mJ K^{-1} mol^{-1}—see Table I). However, for the polycrystalline sample pc1 $\gamma_r = 11.7$ mJ K^{-2} mol^{-1} implying that ~21% of the sample remained in the normal state. Polycrystalline sample pc2 had $\gamma_r=2.3$ mJ K^{-2} mol^{-1}.

The Sommerfeld constants for $B>0$, obtained from the fits using Eq. (3), are composites of $\gamma_r \equiv \gamma(0)$ from normal

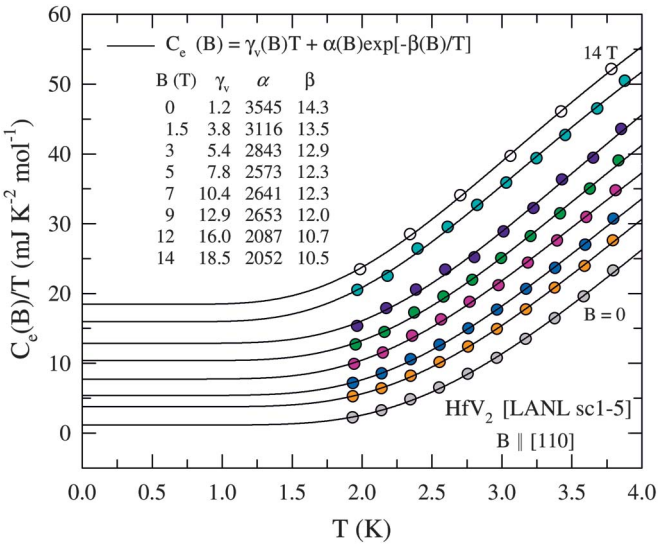

FIG. 14. (Color) A plot of C_{es}/T vs T for the specific-heat data shown is in Fig. 10, which is similar to that of Fig. 13. The fitting expression and parameters are given in the figure. Extrapolations are over longer ranges of temperature than in Fig. 13 because the PPMS cryostat used for the measurements has a limiting lower temperature of ~2 K.

material and $\gamma_v'(B)$ from the vortex state. They are corrected to values corresponding to a fully superconducting sample using the relationship $\gamma_v(B)=[\gamma_v'(B)-\gamma_r]/(1-\gamma_r/\gamma)$ and are plotted in Figs. 15 as $\gamma_v(B)$ vs B. For each cooling sequence through T_M from ambient temperature, a plot of $\gamma_v(B)$ vs B is linear, to within experimental accuracy, but with different slopes $[d\gamma_v(B)/dB]$ and corresponding values of γ—see Table I and Fig. 15. As the number of times cooled from ambient temperature through T_M *increases*, $d\gamma_v(B)/dB$ *decreases*.

If the linear relationship holds to the normal state γ, the extrapolated upper critical fields (B_{c2}) range from 28.6 to 33.6 to 35.4 T for the cooling sequences LBNL sc1-1 and LANL sc1-3,5, respectively. [Because of a malfunction of the PPMS on the fourth cooling (sc1-4), no $B=0$ specific-heat measurements were made, and γ_r was not determined; however, a plot of $\gamma_v'(B)$ vs B—not shown in Fig. 15—was linear.] For a polycrystalline sample of $Hf_{0.4}Zr_{0.6}V_2$, with $T_c=10.1$ K, B_{c2} was reported[23] to be 28 T. ZrV_2 has the same crystal structure as HfV_2 and both undergo martensitic transitions. At 0.005 T an M vs B measurement, where M is the magnetic moment, gave a T_c of 7.7 K for the first cooling through T_M. This is comparable to $T_c=7.78$ K for the first cooling of HfV_2. Consequently, the $B_{c2}(0)=28$ T for $Hf_{0.4}Zr_{0.6}V_2$ is probably similar to that for HfV_2, which provides supporting evidence that $\gamma_v(B)$ vs B is linear to γ.

In the vortex state for a type-II superconductor, for B near the lower critical field (B_{c1}), the theory[24] predicts that $\gamma_v(B)$ versus B will be strongly nonlinear (downward curvature) because of vortex-vortex interactions, and will approach linearity only when $B \gg B_{c1}$. If vortex-vortex interactions are absent, or negligible, $\gamma_v(B)$ vs B is linear.[24]

The magnetic susceptibility of a HfV_2 single crystal was measured as a function of B following zero-field cooling to 1.9 K. A plot of M vs B was linear to ~0.02 T with a minimum at 0.046 T. B_{c1} is estimated to be ~0.02 T, but see Sec. IV D for another estimate using the thermodynamic critical field (B_c). (A more precise value of B_{c1} is not possible from the M vs H measurements since the sample is a single crystal of approximately cubic dimension that is not uniformly magnetized, which would cause inhomogeneous flux penetration and exclusion. Another complication is hysteresis produced by pinning.) However, since the lowest in-field measurement of specific heat for sample sc1-3 was at 0.5 T—more than an order of magnitude greater than the minimum in M vs B at 0.046 T—a departure from linearity for $\gamma_v(B)$ vs B would not be expected, nor was one observed.

D. Thermodynamic critical field (B_c) and related parameters

The thermodynamic critical field is defined for $B=0$ as

$$(V/8\pi)B_c(T)^2 = G_{es}(T) - G_{en}(T) = -\int_0^T [S_{es}(T) - \gamma T]dT, \tag{4}$$

where V is the molar volume and G the Gibbs free energy for the superconducting, G_{es}, and normal, G_{en}, states, respectively. At T_c the free energies of the superconducting and normal states are equal and by setting $G_{es}(T_c)-G_{en}(T_c)=0$ the integration constant is determined. The unit cell contains four HfV_2 molecules and its volume is given as a function of temperature in Table II, from which $V=30.1$ cm^3 mol^{-1}. $G_{es}(T)-G_{en}(T)$ was calculated from the specific-heat data for LBNL sc1-1 ($T_c=8.00$ K and $\gamma=42.1$ mJ K^{-2} mol^{-1}). At $T=0$, $B_c(0)=0.245$ T and the curve of $B_c(T)$ versus T can be fit to within 0.3% to the two-fluid model, parabolic expression

$$B_c(T) = B_c(0)[1-(T/T_c)^2] = 0.245[1-(T/8.00)^2]. \tag{5}$$

Equation (5) is not a good representation for BCS superconductors, but for very strong coupling, as in the present case, $C_{es} \propto T^3$ near T_c (see Fig. 11) and the fit is improved. Unlike $B_{c2}(T)$ vs T and $B_{c1}(T)$ vs T, there is no change in properties when the $B_c(T)$ boundary is crossed. However, it is related to B_{c1} and B_{c2} by characteristic superconducting parameters that are associated with the Ginzburg-Landau theory of superconductivity[25]

$$B_{c2} = (2)^{1/2}\kappa B_c = \Phi_0/2\pi\xi^2 = 4\pi\lambda_p^2 B_c^2/\Phi_0 \tag{6}$$

and

$$B_{c1} \approx [\ln\kappa/(2)^{1/2}\kappa]B_c, \tag{7}$$

where ξ is the coherence length, λ_p the penetration depth, $\kappa \equiv \lambda_p/\xi$ ($\kappa<1$ for type-I and $\kappa>1$ for type-II superconductors), and Φ_0 is the flux quantum (2.07×10^{-11} T cm^2).

Using $B_{c2}(0)=22.6$ T from the extrapolation of $\gamma_v(B)$ vs B for LBNL sc1-1] and $B_c(0)=0.245$ T gave: $\kappa(0)=82$, $\xi(0)=34$ Å, $\lambda_p(0)=2800$ Å, and $B_{c1}(0)\approx0.009$ T. A similar fit to the LANL sc1-5 data ($T_c=8.60$ K and $\gamma=45.9$ mJ K^{-2} mol^{-1}) using the extrapolated $B_{c2}(0)=35.4$ T gave: $B_c(0)=0.279$ T, $\kappa(0)=90$, $\xi(0)=31$ Å, $\lambda_p(0)=2740$ Å, and $B_{c1}(0)\approx0.01$ T. The fit of $B_c(T)$ vs T for LANL sc1-5 to Eq. (5) was similar to that of LBNL sc1-1: $B_c(T)=0.280[1-(T/8.61)^2]$.

The lower critical field, $B_{c1}(0)$, calculated from Eq. (7) is less well determined than the other parameters. Nevertheless, it is not inconsistent with $B_{c1}(0)<0.02$ T estimated from the M vs B measurements at 1.9 K.

The coherence length ξ, is much smaller than the grain size of 1 to 5 microns (10 000 to 50 000 Å) estimated from the x-ray measurements below T_M . Consequently, the proximity effect can not be invoked to explain the presence of a single, sharp anomaly at T_c for a mixture of cubic and orthorhombic phases.

E. The discontinuity in specific heat at T_c

Figure 16 is a plot of C_e/T vs T for the LBNL measurements on sc1 made for $B=0$, where the transition to the superconducting state has a width $\Delta T_c \sim 1$ K. The C_{es}/T data below T_c are corrected and normalized to that for a fully superconducting sample by subtracting $\gamma_r=0.5$ mJ K^{-2} mol^{-1} and dividing by the factor $(1-\gamma_r/\gamma)$. An entropy-conserving construction defines $T_c=8.00$ K and the size of the discontinuity $\Delta C(T_c)/T_c=87.1$ mJ K^{-2} mol^{-1} for an ideal superconducting transition. The scaled discontinuity

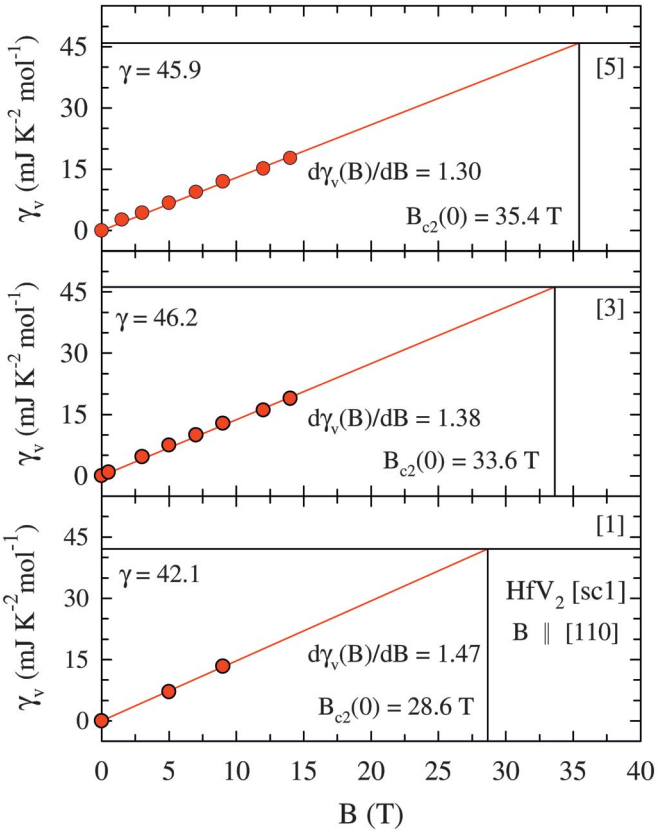

FIG. 15. (Color) Plots of $\gamma_v(B)$ vs B determined for $B\|[110]$ axis. From bottom-to-top the data are from LBNL sc1-1, LANL sc1-3, and LANL sc1-5. While γ_v is linear in B, $\gamma_v(B)$, and $d\gamma_v(B)/dB$ are dependent on the thermal history. The upper critical field (B_{c2}) is evaluated assuming the linear relationship holds to γ. The differences in γ and B_{c2} are probably attributable to different ratios of cubic-to-orthorhombic phases and/or variations of the stress fields developed at the martensitic transition.

at T_c, $\Delta C(T_c)/\gamma T_c = 2.07$, is indicative of strong electron-phonon coupling, which is in accord with the T^3 dependence near T_c shown in Fig. 11. A BCS curve, where $\Delta(T_c)/\gamma T_c = 1.43$, is shown for comparison. Although both T_c and γ are dependent on the cooling sequence for sample sc1 (they range from 7.8 to 9.0 K and 42.1 to 53.8 mJ K^{-2} mol^{-1}, respectively), the values of $\Delta C(T_c)/\gamma T_c$ have a smaller variation—1.95 to 2.10—to within approximately the accuracy of the various measurements—see Table I. Samples sc2, pc1, and pc2 also have $\Delta C(T_c)/\gamma T_c$ values of 1.99, 1.95, and 1.93, respectively. If different samples have different ratios of cubic-to-orthorhombic phases below T_M, this observation supports the argument that superconductivity in HfV_2 is essentially independent of the crystallographic phase.[16,20] [For other polycrystalline samples, reported previously,[10,13–16] $\Delta C(T_c)/\gamma T_c$ ranges from 1.7 to 2.0.] For comparison Pb, which is a strongly coupled type-I superconductor,[26] has $T_c = 7.19$ K and $\Delta C(T_c)/\gamma T_c = 2.65$.

F. Fit of C_{es} to the α model for $B=0$

A semiempirical modification of the BCS formalism, the α model,[27] was developed to enable a quantitative fit of the specific heat of strongly coupled, single-gap superconductors. (This interpretation was recently extended to two-gap superconductors[28] and was successfully applied to MgB_2.) In the α model's phenomenological modification of the BCS theory the superconducting energy-gap ratio, $\Delta(0)/k_BT_c$ (k_B is the Boltzmann constant), is used as a fitting variable in place of the lower-bound BCS value 1.764; however, the temperature dependence of the gap is assumed to be the same

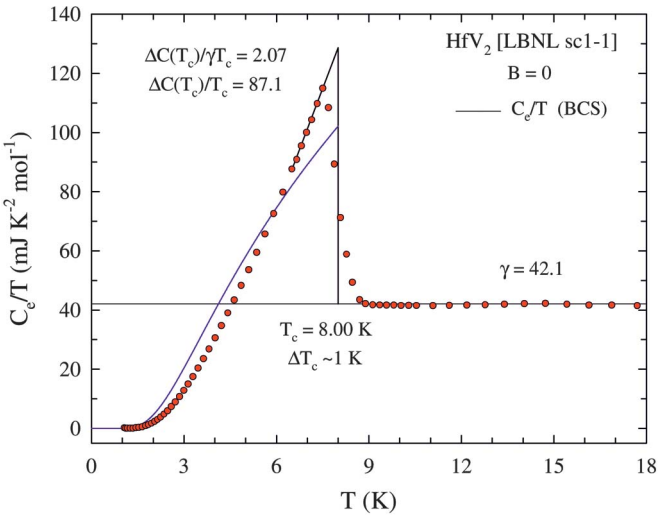

FIG. 16. (Color) A plot of C_e/T vs T for $B=0$, for the larger single-crystal piece (sc1) of HfV_2 measured at LBNL, with an entropy-conserving construction that defines T_c. The data have been corrected, as discussed in the text, for the EDOS of the small amount of assumed normal material. The BCS specific-heat curve is shown for comparison. The increased height of the anomaly, compared to that for a BCS superconductor, indicates strong electron-phonon coupling.

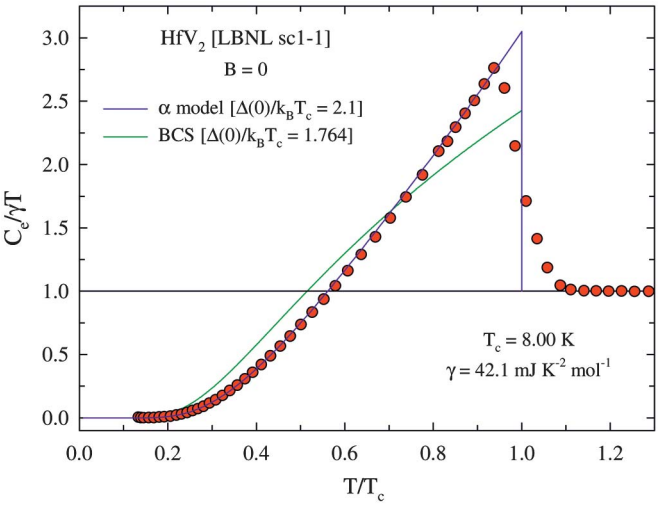

FIG. 17. (Color) This plot illustrates the fit of the LBNL sc1-1 C_{es} data shown in Fig. 16 to the α model, a phenomenological modification of the BCS theory that is applicable to strongly coupled superconductors. The fit is excellent and the superconducting energy-gap ratio of 2.1 is nearly identical to the 2.2 energy-gap ratio for the type-1 superconductor Pb. The BCS curve is included for comparison.

as that of the BCS theory. Figure 17 shows the α-model fit to the LBNL specific-heat data for sc1. The fit uses a gap ratio $\Delta(0)/k_BT_c=2.1$, and it agrees well with the normalized C_{es} data. This energy gap ratio is nearly identical to the 2.2 for Pb.[29] For comparison, the BCS curve is also shown in Fig. 17. The LANL data for sc1, sc2, pc1, and pc2 can also be fit by the α model with very similar results.

G. Electron-phonon coupling constant λ

Band-structure calculations have been reported[30] for HfV_2 in the cubic C15 Laves phase that give a bare density of states at the Fermi level $N_b(E_F)=197.9$ states Ry^{-1} (primitive unit cell)$^{-1}$. Since there are two HfV_2 formula units in a primitive unit cell, $N_b(E_F)=99.0$ states Ry^{-1} $(HfV_2)^{-1}$. The relationships between $N(E_F)$, and the bare density of states γ_b are given by

$$N(E_F)=(1+\lambda)N_b(E_F)=(3/\pi^2k_B)(1+\lambda)\gamma_b=(3/\pi^2k_B)\gamma, \quad (8)$$

where λ is an interaction parameter with electron-phonon and electron-electron coupling components. It can be written as

$$\lambda=(\gamma/\gamma_b-1)=(m^*/m_b-1). \quad (9)$$

Here m_b is the band-structure electron mass modified by the periodic potential and m^* the effective electron mass, increased due to interactions. For the LBNL measurements $\gamma=42.1$ mJ K^{-2} mol^{-1} from which $N(E_F)=5.76\gamma=242$ states Ry^{-1} $(HfV_2)^{-1}$. Using $N_b(E_F)$, from the bare density of states calculation, and $N(E_F)$ in Eq. (8) gives $\lambda=1.45$, which is consistent with HfV_2 being a strongly coupled superconductor. [At low temperatures, where γ is determined, HfV_2 is a mixture of orthorhombic and minority cubic crystallographic phases. Consequently, using the $N_b(E_F)$ calculated for the cubic phase probably results in some inaccuracy for the derived λ.] Values of λ range from 1.61 to 2.13 using γ's evaluated from the LANL measurements on the two single crystals. This variation presumably reflects the effect of strains and/or the amount of untransformed cubic phase. For comparison, λ's for the strongly coupled type-I superconductor Pb are 1.48 from resistivity,[31] 1.55 from tunneling,[32] and 1.68 from a theoretical calculation using a local density approximation (LDA).[33] They are similar to λ's for HfV_2. Table I lists λ values, calculated from previously reported values of γ, and $N_b(E_F)$ from Ref. 30, for polycrystalline samples that range from 1.8 to 2.4. Our polycrystalline sample pc1 has $\lambda=2.25$ and sample pc2 has $\lambda=2.51$. These larger values, relative to those of the single crystals, could be associated with different stress fields, and/or ratios of cubic-to-orthorhombic phases below T_M, and the stoichiometry.

McMillan[34] introduced an equation that relates T_c, Θ_D, and λ that is applicable to conventional electron-phonon coupled superconductors when $\lambda \lesssim 1.5$,

$$T_c=(\Theta_D/1.45)\exp\{-1.04(1+\lambda)/[\lambda-\mu^*(1+0.65\lambda)]\}, \quad (10)$$

where μ^* is the "renormalized" Coulomb repulsion. Values of μ^* are not well defined; and, it is usually assumed that $\mu^* \leqslant 0.2$, but there is evidence that it can be larger.[35] In the derivation of Eq. (6) McMillian used the phonon spectrum for Nb, which is characteristic of a number of conventional superconductors. His formula was later modified by Allen and Dynes[36] who replaced the $\Theta_D/1.45$ prefactor with a more correct $\omega_{ln}/1.20$, where ω_{ln} is a moment of the phonon frequencies weighted by electron-phonon matrix elements. (Unlike Θ_D, however, a value for ω_{ln} is not easily obtained.) Using the parameters derived from the LBNL measurements in Eq. (10)—$\Theta_D=177$ K, $T_c=8.00$ K, $\lambda=1.45$—the renormalized Coulomb repulsion $\mu^*=0.27$. On the other hand, if the Allen and Dynes modification of Eq. (10) is used with $\mu^*=0.1$, $\omega_{ln}=72$ K. There is a simple relationship[37] between T_c, ω_{ln}, and λ_{eff} expressed as

$$T_c=0.25\omega_{ln}/[\exp(2/\lambda_{eff})-1]^{1/2}, \quad (11)$$

where $\lambda_{eff} \approx \lambda/(1+2.6\mu^*)$ for $\lambda>1$. It follows from Eq. (11) that the ratio T_c/ω_{ln} is a measure of the coupling strength. In the present case, for $\mu^*=0.1$, $T_c/\omega_{ln}=0.11$, which is essentially equal to the ratio 0.10 for Pb.[37]

V. CONCLUSIONS

In summary, HfV_2 is a strongly coupled type-II superconductor whose energy gap and electron-phonon coupling strength are very similar to Pb, a strongly coupled type-I superconductor. The superconductivity is not unconventional as was suggested in some previous work. The α model, a phenomenological modification of the BCS theory that is applicable to strongly coupled superconductors, can be used to fit the LBNL sc1-1 data for $B=0$ to within experimental accuracy, with a superconducting energy-gap ratio $\Delta(0)/k_BT_c=2.1$. Similar fits and agreements with data can be made for the LANL measurements.

Parameters characterizing the specific heat of HfV_2 for the single crystals are dependent on the number of thermal cycles from ambient temperature through the martensitic transition at $T_M=117.6$ K. Evidence for this is the dependence of T_c, γ, γ_r, and C_{lat} on the thermal history; however, there is very little effect on the ratio $\Delta C(T_c)/\gamma T_c$. The successive cooling of HfV_2 from ambient to low temperatures causes a general increase in γ that is coupled to the increases in T_c, which approach 9.0 K, perhaps a limiting value.

Structural x-ray determinations showed that the high-temperature cubic phase was not transformed completely to the low-temperature orthorhombic phase at T_M and that the amount for sample sc3 (ground into a powder for the measurements) was unchanged in magnitude at ~9 wt. % when successively cooled from 140 K. Such an incomplete conversion of phases is commonly observed in martensitic transitions, and is usually sample dependent. Because of the incompleteness of the transition, it seems plausible that the dependence of the specific heat on thermal history is a result of changes in the ratio of untransformed cubic-to-orthorhombic phases and/or strains developed at T_M. If the ratio of cubic-to-orthorhombic phases is relatively reproducible for repeated cycling through T_M from ambient temperature the progressive increase of T_c—and changes in other parameters—can be rationalized assuming "training" of the sample, which occurs via the elongation of the orthorhombic c axis, thus reducing strain below T_M.

DSC measurements demonstrate that the transition hysteresis is ~1 K for successive warming/cooling cycles between 90 and 140 K, with no additional effects on T_M. Furthermore, they confirm that the martensitic transition to the orthorhombic phase is incomplete.

Both the cubic and orthorhombic phases are superconducting since there is only a small, residual γ_r that is assumed to be associated with an EDOS for a normal-state phase of HfV_2. Since there is a single, relatively sharp, superconducting anomaly the two phases must have nearly identical T_c's and be affected similarly by the thermal history. The relatively large grain size, in the low micron range, and the small coherence length ξ=31 Å preclude the proximity effect as a mechanism for producing a single anomaly. We speculate that the same T_c values observed for each phase arise from the fact that the V tetrahedra leave the phonons associated with the superconductivity unchanged.

In the vortex state $\gamma_v(B)$ is linear in B; however, $d\gamma_v(B)/dB$ and $B_{c2}(0)$, evaluated from an extrapolation to γ, depend on the thermal history, and change monotonically with the number of cycles from ambient temperature through T_M.

ACKNOWLEDGMENTS

The work at LANL was supported by the United States Department of Energy under Grant No. DEFG-03-86ER-45230, the U.S. National Science Foundation (NSF) under Grant No. DMR-00-72125, and was performed under the auspices of the NSF, the State of Florida, the National Nuclear Security Administration, and the U.S. Department of Energy. The work at Lawrence Berkeley National Laboratory was supported by the Director, Office of Basic Energy Sciences, Materials Sciences Division of the U.S. Department of Energy under Contact No. DE-AC03-76SF00098. The work at Ames Laboratory was supported by the Materials Sciences Division of the Office of Basic Energy Sciences under Contract No. W-7405-ENG-82. The authors thank A. Lawson and T. Finlayson for informative discussions.

[1] B. T. Matthias, T. H. Geballe, and V. B. Compton, Rev. Mod. Phys. **35**, 414 (1963).
[2] V. Sadagopan, E. Pollard, and H. C. Gatos, Solid State Commun. **3**, 97 (1965).
[3] K. Inoue, K. Tachikawa, and Y. Iwasa, Appl. Phys. Lett. **18**, 123 (1971).
[4] T. F. Smith, R. N. Shelton, and A. C. Lawson, J. Phys. F: Met. Phys. **3**, 157 (1973).
[5] M. Tenhover, Appl. Phys. Lett. **21**, 279 (1980).
[6] Y. A. Izyumov, V. E. Naish, and V. N. Syromyatnikov, Sov. Phys. Crystallogr. **21**, 137 (1976).
[7] R. Heidinger, H. Appel, G. Then, and W. G. Thies, Phys. Status Solidi A **121**(2), 445 (1990).
[8] T. R. Finlayson, E. J. Lanston, M. A. Simpson, E. E. Gibbs, and T. F. Smith, J. Phys. F: Met. Phys. **8**, 2269 (1978).
[9] F. Chu, M. Sob, R. Siegl, T. E. Mitchell, D. P. Pope, and S. P. Chen, Philos. Mag. B **70**, 881 (1994).
[10] P. Rapp and L. J. Vieland, Phys. Lett. **36A**, 369 (1971).
[11] Y. Kimura, J. Phys. Soc. Jpn. **36**, 306 (1974).
[12] J. W. Hafstrom, G. S. Knapp, and A. T. Aldred, Phys. Rev. B **17**, 2892 (1978).
[13] B. Lüthi, M. Herrmann, W. Assmus, H. Schmidt, H. Rietschel, H. Wühl, U. Gottwick, G. Sparn, and F. Steglich, Z. Phys. B: Condens. Matter **60**, 387 (1985).
[14] Y. Kishimoto, N. Shibata, T. Ohno, Y. Kitaoka, K. Ayasama, K. Amaya, and T. Kanashiro, J. Phys. Soc. Jpn. **61**, 696 (1992).
[15] F. Chu, Z. W. Chen, C. J. Fuller, C. L. Lin, and T. Mihalisin, J. Appl. Phys. **79**, 6405 (1996).
[16] M. J. Parsons, P. J. Brown, J. Crangle, K.-U. Neumann, B. Ouladdiaf, T. J. Smith, N. K. Zayer, and K. R. A. Ziebeck, J. Phys.: Condens. Matter **10**, 8523 (1998).
[17] A. P. Holm, V. K. Pecharsky, K. A. Gschneidner, Jr., R. Rink, and M. Jirmanus, Rev. Sci. Instrum. **75**, 1081 (2004).
[18] J. Marcos, F. Casanova, X. Batlle, A. Labarta, A. Planes, and Ll. Mañosa, Rev. Sci. Instrum. **167**, 4778 (2003).
[19] Y. Zhao, F. Chu, R. B. Von Dreele, and Q. Zhu, Acta Crystallogr., Sect. B: Struct. Sci. **B56**, 601 (2000).
[20] S. Dressler, J. W. Taylor, B. Ouladdiaf, K.-U. Neumann, and K. R. A. Ziebeck, Solid State Commun. **113**, 649 (2000).
[21] J. Bardeen, L. N. Cooper, and J. R. Schrieffer, Phys. Rev. **108**, 1175 (1957).
[22] J. Bardeen and J. R. Schriffer, in *Progress in Low Temperature Physics III*, edited by Gorter (North-Holland, Amsterdam, 1961), Vol. 170, p. 212.
[23] K. Inoue and K. Tachikawa, IEEE Trans. Magn. **13**, 840 (1977).
[24] K. Maki, Phys. Rev. **139**, A702 (1965); A. L. Fetter and P. C. Hohenberg, in *Superconductivity*, edited by R. D. Parks (Dekker, New York, 1969).
[25] M. Tinkham, *Introduction to Superconductivity* (McGraw-Hill, New York, 1996).
[26] G. Rickayzen, in *Theory of Superconductivity*, Monographs and Texts in Physics and Astronomy XIV, edited by R. E. Marshak (Wiley/Interscience, London, 1965), p. 205.
[27] H. Padamsee, J. E. Neighbor, and C. A. Shiffman, J. Low Temp. Phys. **12**, 387 (1973).
[28] F. Bouquet, Y. Wang, R. A. Fisher, D. G. Hinks, J. D. Jorgensen, A. Junod, and N. E. Phillips, Europhys. Lett. **56**, 856 (2001).
[29] P. L. Richards and M. Tinkham, Phys. Rev. **119**, 575 (1960); P. Townsend and J. Sutton, *ibid.* **128**, 591 (1962).
[30] A. Ormeci, F. Chu, J. M. Wills, T. E. Mitchell, R. C. Albers, D. J. Thoma, and S. P. Chen, Phys. Rev. B **54**, 12753 (1996).
[31] P. B. Allen, Phys. Rev. B **36**, 2920 (1987).
[32] W. L. McMillan and J. M. Rowell, Phys. Rev. Lett. **19**, 108 (1965).
[33] S. Y. Savrasov and D. Y. Savrasov, Phys. Rev. B **54**, 16487 (1996).
[34] W. L. McMillan, Phys. Rev. **167**, 331 (1968).
[35] P. B. Allen, in *Handbook of Superconductivity*, edited by C. D. Poole, Jr. (Academic Press, New York, 1999) Chap. 9, Sec. G, p. 478.
[36] P. B. Allen and R. C. Dynes, Phys. Rev. B **12**, 905 (1975).
[37] V. Z. Kresin, H. Morawitz, and S. A. Wolf, *Mechanisms of Conventional and High T_c Superconductivity* (Oxford University Press, Oxford, 1993), p. 29.